A 10-year climatology of cloud cover and vertical distribution derived from both surface and GOES observations over the DOE ARM SGP Site

Baike Xi[1], Xiquan Dong[1], P. Minnis[2], M. Khaiyer[2]

[1]University of North Dakota, Grand Forks, ND

[2]NASA Langley Research Center, Hampton, VA

Short title: Temporally and spatially averaged clouds

Abstract

Analysis of a decade of ARM radar-lidar and GOES observations at the SGP site reveal that 0.5 and 4-hr averages of the surface cloud fraction correspond closely to 0.5° and 2.5° averages of GOES cloudiness, respectively. The long-term averaged surface and GOES cloud fractions agree to within 0.5%. Cloud frequency increases and cloud amount decreases as the temporal and spatial averaging scales increase. Clouds occurred most often during winter and spring. Single-layered clouds account for 61.5% of the total cloud frequency. There are distinct bimodal vertical distributions of clouds with a lower peak around 1 km and an upper one that varies from 7.5 to 10.8 km between winter and summer, respectively. The frequency of occurrence for nighttime GOES high-cloud tops agree well with the surface observations, but are underestimated during the day.

1. Introduction

In current climate models, the representation of clouds is a major source of uncertainty [e.g., *Wielicki et al., 1995*]. The vertical distribution of clouds impacts the vertical heating/cooling rate profile by radiative and precipitative/evaporative processes. The assumed or computed cloud vertical profiles in General Circulation Models (GCMs) are one of the main reasons why the different models predict a wide range of future climates [*Stephens et al., 2002*]. For example, the majority of GCMs can only simulate 30-40% of the middle-high cloud observed in the mid-latitudes by satellites, and half of the GCMs underestimate low cloud cover, while none overestimates it [*Zhang et al., 2005*]. Also, it is well known that surface observers can see most of the low clouds with/without higher clouds above them [e.g., *Warren et al., 1984*], while satellites can observe most of the high clouds with/without lower clouds underneath [e.g., *Chang and Li, 2005*]. Thus, it will introduce some ambiguities when the surface and satellite observations are used to derive cloud fractions to validate the model results.

47 The nearly continuous observations by the DOE ARM Program [*Ackerman and Stokes, 2003*] cloud
48 radar-lidar systems can provide more accurate cloud vertical distributions and compensate for most of the
49 shortcomings from both surface observers and satellite imagery. However, the limitation of such
50 observing systems is that they view only a small column of the atmosphere above the instruments
51 providing only a pencil beam. How accurately the surface-based narrow point-of-view observations
52 represent the large grid boxes used in GCMs remains an unresolved issue [*Mace and Benson-Troth,*
53 *2002*] that needs to be addressed before these valuable data can be reliably used to validate GCMs cloud
54 statistics.

55 This paper documents fundamental statistical information about cloud coverage and vertical
56 distribution using a decade of nearly continuous combined radar and lidar data taken from January-1997
57 through December-2006 at the ARM Southern Great Plains (SGP) site and spatially matched cloud
58 retrievals from GOES-8/10 (hereafter GOES) taken from May-1998 through December-2006. The
59 integrated surface-satellite observations allow us to investigate the following two scientific questions:

60 1) Under what conditions (temporal averages) can the point-of-view ARM observations represent
61 the large-scale grid boxes of satellite observations?
62 2) What is the long-term and seasonal climatology of cloud vertical distributions over the ARM
63 SGP site?

64 **2. Data and methods**

65 The ARM 35-GHz Millimeter Wavelength Cloud Radar (MMCR) provides continuous profiles of
66 radar reflectivity from hydrometeors moving through the radar FOV, allowing the identification of clear
67 and cloudy conditions. Cloud-top height (Z_{top}) is derived from MMCR reflectivity profiles with 90-m
68 uncertainty. The lowest cloud-base height (Z_{base}) is derived from a composite of Belfort laser ceilometer,
69 Micropulse Lidar (MPL), and MMCR data [*Clothiaux et al., 2000*]. The cloud fraction (CF) derived from

70 the upward-looking narrow view radar-lidar pair of measurements is simply the percentage of returns that
71 are cloudy within a specified sampling time period, i.e., the ratio of the number of hours when clouds
72 were detected to the total number of hours when both radar and lidar/ceilometer instruments were
73 working. The vertical distributions of CF above the lowest cloud base are the percentage of returns that
74 are cloudy within a specified vertical resolution (90 m in this study) during the 10-yr period.
75 Cloud properties were retrieved from half-hourly, 4-km visible and infrared radiances taken by GOES
76 using the 4-channel VISST (Visible Infrared Solar-Infrared Split-window Technique) for daytime and the
77 3-channel Solar-infrared Infrared Split-window Technique [SIST] for nighttime [*Minnis et al.*, 2001]. The
78 areal fraction of clouds is the ratio of the number of pixels classified as cloudy to the total number of
79 pixels within a specified area (0.5^{o}x0.5^{o}, 2.0ºx2.5º in this study). The technique for determining effective
80 cloud height (H_{eff}) is to estimate effective cloud temperature (T_{eff}) based on the IR radiance adjusted
81 according to cloud optical depth first, and then H_{eff} is defined as the lowest altitude having T_{eff} in the
82 vertical profile of atmospheric temperature. The profile is constructed in three parts. The Rapid Update
83 Cycle (RUC) numerical weather analysis model [*Benjamin et al.*, 2004] profile is used for pressures
84 p<500 hPa. The profile for p>700 hPa is specified using a -7.1 K/km lapse rate anchored to the 24-h
85 running mean surface temperature from the RUC, while a linearly weighted blend of the RUC and lapse
86 rate is used for intermediate pressures. The FREQ is 0 for clear sky and 1 when AMT > 0. The monthly
87 averaged AMT is the average of all AMTs (>0 only). The average FREQ is the ratio of the number of
88 times AMT>0 to the total number of satellite observations during that month. Finally, the monthly mean
89 CF is defined as the product of the monthly averaged AMT and FREQ. Note that FREQ and AMT are
90 fundamental variables for representing cloud occurrence either in a certain time period (e.g. hour, month,
91 etc) or over an area of a particular size (e.g., 0.5ºx0.5º, 2.0ºx2.5º). FREQ represents the probability of how

often the cloud appears within either the time period or area, and CF represents how much area the clouds cover for the same specified temporal and spatial domains.

3. Comparison of clouds observed/derived by ARM and GOES

Since there are significant temporal and spatial differences between surface and satellite observations, comparisons between them must be conducted carefully. If they are statistically representative of a larger area, then the temporally averaged surface observations should be equivalent to the spatially averaged satellite results, assuming that there are enough samples and the satellite and surface instruments are equally efficient at detecting cloudiness. By varying the temporal and spatial resolutions, it should be possible to determine the time and space scales that can be represented by the point measurements. Therefore, we develop the following conceptual model:

$$\lim_{area \to 0} f(area) = f(point)$$
$$\int_0^X f(time) = f(area) \quad (1)$$

where f represents any function, which can be FREQ or AMT. If the ARM data are used as ground truth, then the spatial domain of the GOES observations should be as small as possible and, vice versa, the surface observations should be averaged over a certain time period (X hours, Eq. 1) to match a relatively large grid box of satellite observations.

Figure 1a, 1b, and 1c show the variations of FREQ, AMT, and CF with temporal resolution. The FREQ rises rapidly with increased temporal averaging periods from the 5-min (51%) to 6-hour (92%) intervals. This is reasonable because the possibility of cloud occurrence over a longer time period is certainly higher than that over a short time period at a fixed point, but it may not be true for AMT. The AMT decreases with the increased averaging periods from 87% at 5-min to 49% at 6-hour due to the characteristic of point observations. The CF, however, is almost constant for different temporal resolutions as shown in Figure 1c. To provide more detailed information for climate modelers, the

114 empirical formulae were derived to relate FREQ and AMT to temporal resolution X (hr) shown on Figure
115 1a and 1b.

116 The FREQ, AMT, and CF derived from the 0.5^{o}x0.5^{o} and 2.0^{o}x2.5^{o} GOES grid boxes are also plotted
117 in Figure 1d to 1i. The 0.5^{o} FREQ and AMT agree very well with the 0.5-hr ARM observations, while
118 those derived from the 2.5^{o} region are nearly the same as the 4-hr surface averages. The GOES CFs
119 derived from both boxes are in excellent agreement with the different temporal averages of surface
120 observations (Figure 1f and 1i). This result indicates that the long-term CFs derived from different
121 temporal resolutions can represent the areal CFs with different grid boxes as long as the same geographic
122 feature inside the entire grid box.

123 To further analyze the spatial and temporal relationships, the 0.5-hr and 4-hr surface averages are
124 plotted against the 0.5^{o} and 2.5° GOES means in Figure 1d to 1i. Each point in Figure 1d to 1i represents
125 a monthly mean between May 1998 and December 2006 when both surface and satellite data are
126 available. The monthly mean surface-derived FREQ and AMT are highly correlated with their respective
127 GOES means and, on average, differ from the satellite means by no more than ±1.5%. The mean
128 difference in FREQ between the 4-hr surface average and 2.5^{o} satellite result is small, but the correlation
129 is relatively weak, presumably due to a small dynamic range (70-98%). All of the monthly mean CFs in
130 Figure 1f and 1i are nearly the same, and the surface and satellite values are highly correlated. This figure
131 again demonstrates that the CF is independent of temporal resolution and the size of grid box for this
132 region.

133 The comparisons in Figure 1 beg the question: what point observations can be directly compared with
134 satellite observations? As shown in Figures 1c, 1f, and 1i, the CF is independent of temporal and spatial
135 resolutions, and the surface-derived CF (a pencil beam) can represent the satellite-derived CF (a grid box)
136 as long as there are enough samples. However, the surface-derived AMT and FREQ cannot be directly

compared with satellite results; they must be averaged over a certain time period to match a fixed grid box of satellite observations.

4. Cloud vertical distributions

Figure 2 shows the annual and seasonal mean vertical distributions of CF derived from the radar-lidar measurements during the 10-yr period. As demonstrated in Figure 2, the single- and multilayered clouds at the annual and seasonal scales have similarly shaped vertical distributions, and they differ by only 2-3% (more single-layered clouds) at a given altitude. Note that the total CF has a relatively large seasonal variation with a maximum in winter and a minimum in summer. There is a distinct bimodal vertical distribution of clouds with a lower peak between 0.8 and 1.8 km and a higher one between 7.5 and 10.8 km. The minimum CF occurs above the boundary-layer inversion at about 2-3 km. The maximum CFs for both the lower and higher peaks occur during winter. The maximum total, single-, and multi-layered CFs are 14.8%, 8.7%, and 6.1%, respectively, for the higher peak; and they are 12.5%, 7.4%, and 5.1%, respectively, for lower peak. The greatest altitude of the upper-level maximum occurs around 10.8 km during summer as a result of a deeper troposphere and more convective storms. The low-level relative maximum during summer is not as strong as those during other seasons because stratus clouds are least common during the summer. The lower and upper peaks during spring and fall are the same as those for the annual vertical distributions, and are located at ~1.3 and 8.8 km, respectively.

To evaluate the satellite-derived cloud vertical distributions, the highest effective cloud-top distributions retrieved from the GOES data are compared in Figure 3 with the ARM radar-derived maximum and all cloud tops over the SGP site during the study period. The cloud top frequency of occurrence and fractional coverage were computed for every 0.25 km in the vertical. During daytime (Figure 3a), the satellite-derived high clouds occur much less frequently than the surface-retrieved high clouds, while middle and low clouds from GOES are found more often than those from the surface. The

160 frequency of the nighttime GOES high-cloud tops (Figure 3b) is in excellent agreement with the
161 maximum high-cloud tops from the surface observations, but the low clouds occur more often than their
162 surface-observed counterparts. The relationships between the ARM and GOES high and middle cloud
163 fractions during both day (Figure 3c) and night (Figure 3d) are similar to those for their frequencies of
164 occurrence, but those relationships differ significantly for the low clouds. The daytime distribution of
165 low-cloud fraction from GOES is similar to that for the ARM for the all clouds, with a slight
166 underestimation in integrated height over the bottom 3 km of the profile. At night, the integrated low
167 cloud fraction is in better agreement with the maximum cloud top values but with a slightly larger
168 underestimate than during daytime.

169 The greater frequency and fractional coverage of middle clouds from GOES relative to the ARM
170 data during daytime are primarily due to three factors. First, H_{eff} is the retrieved radiating height of the
171 cloud, not the physical cloud top. For thick and thin ice clouds, the effective radiating height is generally
172 deep within the cloud, so differences of 1-2 km are expected in many cases [e.g., *Minnis et al.,* 1991,
173 *Minnis et al.,* 2008c]. Second, the ice cloud optical depth from the VISST tends to be overestimated for
174 semitransparent clouds [*Min et al.*, 2004], so that the cloud radiating temperature (height) will be
175 overestimated (underestimated) for thin cirrus. Third, during daytime, thin cirrus over a low cloud will be
176 interpreted as a midlevel cloud with H_{eff} primarily dependent on the optical depth of the upper cloud. The
177 relatively large difference between GOES and SFC MAX at 4 km in Figure 3c suggests that most of the
178 cirrus over low clouds is optically thin.

179 At night, the shapes of the GOES cloud occurrence (Figure 3b) and fraction (Figure 3d) vertical
180 distributions are similar to their ARM counterparts except that the high (midlevel) cloud fractions are less
181 (greater) than the SFC MAX values. This change from the daytime relationships is primarily due to the
182 use of infrared channels only in the SIST. The sensitivity to particle shape in the visible channel retrieval

183 of optical depth, which is the likely source of the overestimate during the day, is gone at night resulting in
184 more accurate thin cirrus optical depths and H_{eff}. The height of the thin cirrus over low clouds at night is
185 also expected to be much higher than during the day, when the visible optical depth in those conditions is
186 high and no adjustment is made for semi-transparency. At night, the retrieved optical depth depends on
187 the difference between the high and low cloud temperatures, which is close to that between the high cloud
188 and the surface. Thus, the retrieved cloud tops are often close to the single-layer case and, subsequently,
189 the GOES midlevel cloud fraction is much closer to SFC MAX than during daytime. These day-night
190 differences are consistent with the single-layer height comparisons performed by *Smith et al.* [2008].
191 The vertical profiles of GOES low cloud occurrence frequencies and fractions change significantly.
192 Although the FREQ is quite large for the lowest height bins, the AMT is small resulting in a peak at 1.38
193 km during daytime and a more uniform fraction distribution at night. The small values of AMT and large
194 values of FREQ in the lowest bin could be due to small cumulus clouds or fog patches during the day and
195 fog patches and noise in the brightness temperature differences at night. The latter would result in small
196 cloud amounts with temperatures close to the surface value. *Dong et al.* [2008] and *Smith et al.* [2008]
197 found that the average VISST low-cloud top heights were 0.1 to 0.5 km less than the radar values, results
198 that are similar to those in Figure 3.

199 **5. Summary and Concluding remarks**

200 Analysis of a decade of nearly continuous ARM radar-lidar and GOES satellite observations at the
201 ARM SGP site has yielded the following conclusions.

202 1) There is excellent agreement in long-term mean CFs determined from the surface and GOES. The CF
203 is independent of temporal resolution and spatial scales, at least, up to the size of a 2.5° grid box
204 providing there are enough samples. FREQ is increased and AMT is decreased with increasing
205 temporal and spatial scale. When computed over a 0.5-hr period, FREQ, AMT, and CF derived from

206 the surface data agree well with the same quantities determined from GOES for a 0.5° region centered
207 on the site. Similarly, the 4-hr surface averages are comparable to those derived from GOES for a 2.5°
208 grid box. Thus, when comparing clouds from weather/climate models to the SGP cloud data, the
209 temporal average time should be matched to the size of the areal resolution. Empirical functions
210 developed here for that purpose are unlikely to be useful for model regions much larger than 2.5°
211 because that is the upper limit of regional size that was considered.

212 2) From ARM radar-lidar data, the vertical distributions of total/single-/multi-layered clouds during all
213 seasons are distinct bimodal with a lower peak (~1 km) and an upper one between 7.5-10.8 km,
214 respectively, as the troposphere expands. Minimum CF occurs within 2-3 km. There are 1.6 times of
215 more single-layered than multilayered clouds at the SGP site during the study period. The 10-year
216 mean total CF, 46.9%, varies seasonally from a minimum 39.8% (summer) to a maximum 54.6%
217 (winter). The vertical distribution of nighttime GOES high-cloud tops agrees well with surface
218 observations, but during daytime, there fewer high clouds than seen from the surface observations. The
219 FREQ for both daytime and nighttime GOES low cloud tops are significantly higher than surface
220 observations, but the CFs are in good agreement.

221 These results should provide the most reliable statistics, to date, of the long-term average vertical
222 distributions of clouds over the climatically important SGP site. These statistics can be used as cloud truth
223 for both surface observers and satellite researchers to quantitatively understand and explain the
224 differences between their observations and cloud truth. They should be also valuable for advancing our
225 understanding of the vertical distributions of clouds and for enabling climate/forecast modelers to more
226 fully evaluate their simulations and improve their parameterizations over the SGP site. The comparisons
227 between the satellite and surface data indicate the areas of needed improvement in the satellite retrievals.
228 The results shown here represent only one region on the globe and may not necessarily represent the

229 spatial and temporal interchangeability of cloud cover in other areas, such as coastal stations where long-
230 term spatial gradients are likely.

231 ***Acknowledgements:***

232 Thanks to Sally Benson and Gerald G. Mace of the University of Utah for providing preprocessed ARM
233 data. This research was primarily supported by the NASA MAP project under Grant NNG06GB59G at
234 the University of North Dakota(UND) and by the Office of Science (BER), U.S. Department of Energy,
235 Interagency Agreement No. DE-AI02-08ER64546. The UND authors were also supported by the NASA
236 CERES project under Grant NNL04AA11G, the NASA NEWS project under Grant NNX07AW05G,
237 and NSF under Grant ATM0649549.

238 **References**

239 Ackerman, T. P., and G. M. Stokes (2003), The ARM Program, *Physics Today*, ***56,*** 38-44.

240 Benjamin, S. G., et al., An hourly assimilation/forecast model: The RUC, *Mon. Wea. Rev.*, ***113***, 495-518.

241 Chang, F., and Z. Li (2005), A near-global climatology of single-layer and overlapped clouds and their
242 optical properties from Terra/MODIS data using a new algorithm, *J. Clim.,* **18**, 4752-4771.

243 Clothiaux, E.E., and coauthors (2000), Objective determination of cloud heights and radar reflectivities
244 using a combination of active remote sensors at the ARM CART sites, *J. Appl. Meteor.*, ***39***, 645-665.

245 Dong, X., P. Minnis, B. Xi, S. Sun-Mack, and Y. Chen, 2008: Comparison of CERES-MODIS stratus
246 cloud properties using ground-based measurements at the DOE ARM SGP site. *J. Geophys. Res.*,
247 ***113***,D03204,doi:10.1029/2007JD008438.

248 Mace, G.G. and S. Benson-Troth (2002), Cloud-layer overlap characteristics derived from long-term
249 cloud radar data, *J. Clim.*, ***15***, 2505-2515.

250 Min, Q, P. Minnis, and M. M. Khaiyer (2004), Comparison of cirrus optical depths from GOES-8 and
251 surface measurements, *J. Geophys. Res.*, ***109***, D20119, 10.1029/2003JD004390.

252 Minnis, P., P. W. Heck, and E. F. Harrison (1990), the 27-28 October 1986 FIRE IFO Case Study: Cloud
253 parameter fields derived from satellite data, *Mon. Wea. Rev.*, ***118***, 2426- 2446.

254 Minnis, P., and Co-authors (2001), A near real-time method for deriving cloud and radiation properties
255 from satellites for weather and climate studies. *Proc. 11th AMS Conf. Satellite Oceanogr. and*
256 *Meteorol.*, Madison, WI, Oct. 15-18, 477-480.

257 Minnis, P., C. Yost, S. Sun-Mack, and Y. Chen (2008c), Estimating the top altitude of optically thick ice
258 clouds from thermal infrared satellite observations using CALIPSO data, *Geophys. Res. Lett.*, **35**,
259 L12801, doi:10.1029/2008GL033947.

Smith, W. L., P. Minnis, H. Finney, R. Palikonda, and M. M. Khaiyer (2008), An evaluation of operational GOES-derived single-layer cloud top heights with ARSCL over the ARM Southern Great Plains site, *Geophys. Res. Lett.*, ***35***, L13820, doi:10.1029/2008GL034275.

Stephens, G.L., and coauthors (2002), The cloudsat mission and the A-train, *Bull. Amer. Meteor. Soc.*, **83**, 1771-1790.

Warren, S.G., C.J. Hahn, J. London, R.M. Chervin, and R.L. Jenne, (1984), Atlas of simultaneous occurrence of different cloud types over land. NCAR Tech. Note, *NCAR/TN-241+STR,* 209 pp., Natl. Cent. for Atmos. Res., Boulder, Colo.

Wielicki, B.A., R.D. Cess, M.D. King, D.A. Randall, and E.F. Harrison (1995), Mission to Planet Earth: Role of clouds and radiation in climate, *Bull. Amer. Meteor. Soc.*, ***76***, 2125-2153.

Zhang, M.H. and coauthors (2005), Comparing clouds and their seasonal variations in 10 atmospheric genergal circulation models with satellite measurements. *J. Geophys. Res.,* ***110,*** D15S02, doi:10.1029/2004JD005021.

Figure 1. Dependence of (a) FREQ, (b) AMT and (c) CF on temporal resolution of radar/lidar observations, and on grid boxes of satellite observations at the SGP site; Scatter plots of monthly means (d) FREQ, (e)AMT, and (f) CF derived from GOES (0.5^ox0.5^o box) and ARM radar/lidar observations; (g) FREQ, (h) AMT, and (i) CF are same as (d), (e), (f) except GOES used 2^ox2.5^o box.

Figure 2. Mean vertical distributions of (a) total, (b) single-layer, and (c) multilayer CF derived from the radar-lidar measurements with a 90-m vertical resolution at the SGP site, 1997-2006.

Figure 3. Comparison of cloud-top distributions and fractions retrieved from GOES and from SGP radar-lidar data over the SGP. 199805-200612.

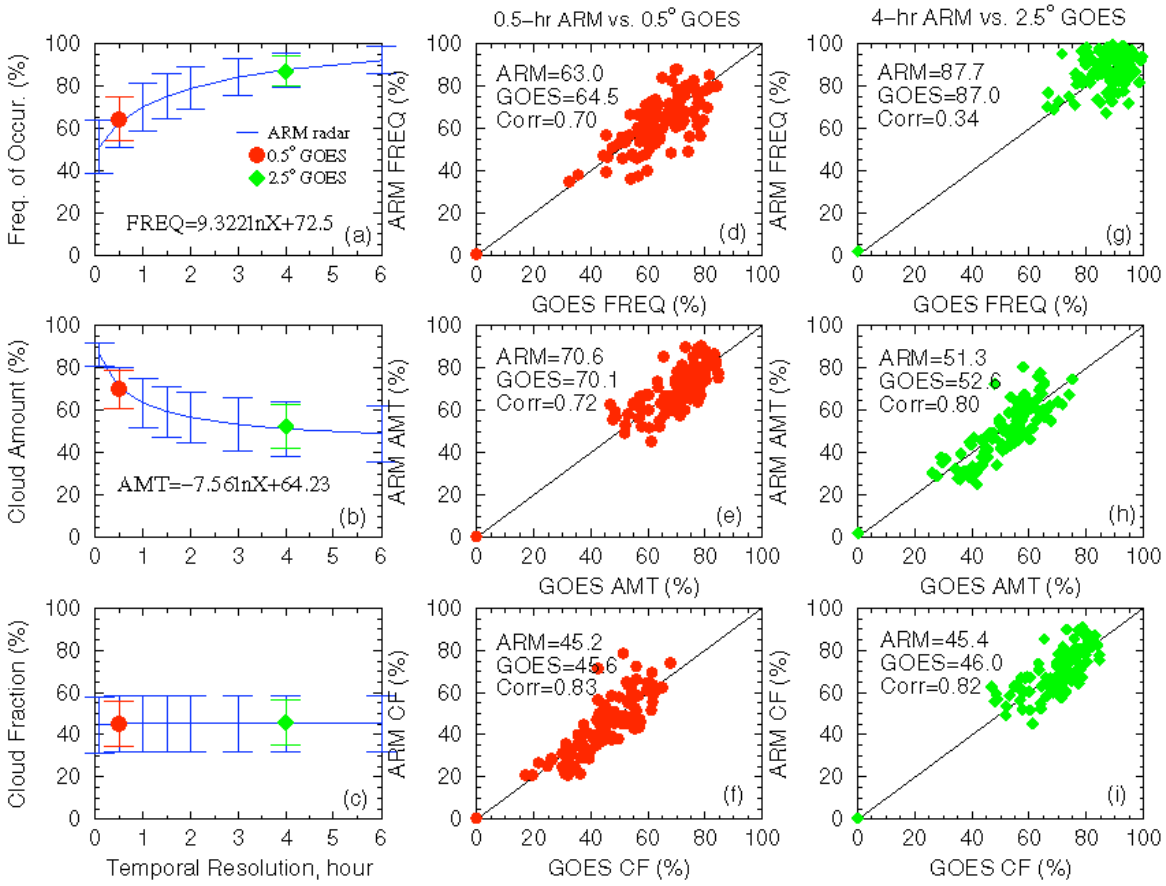

283

284 Figure 1.

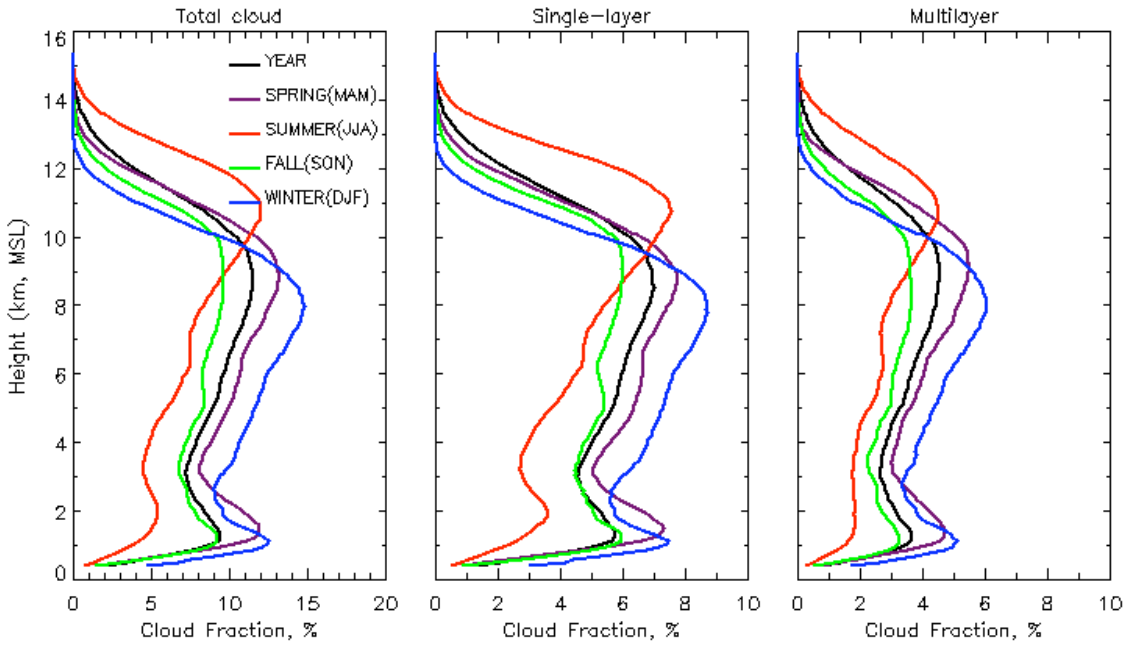

285

286 Figure 2.

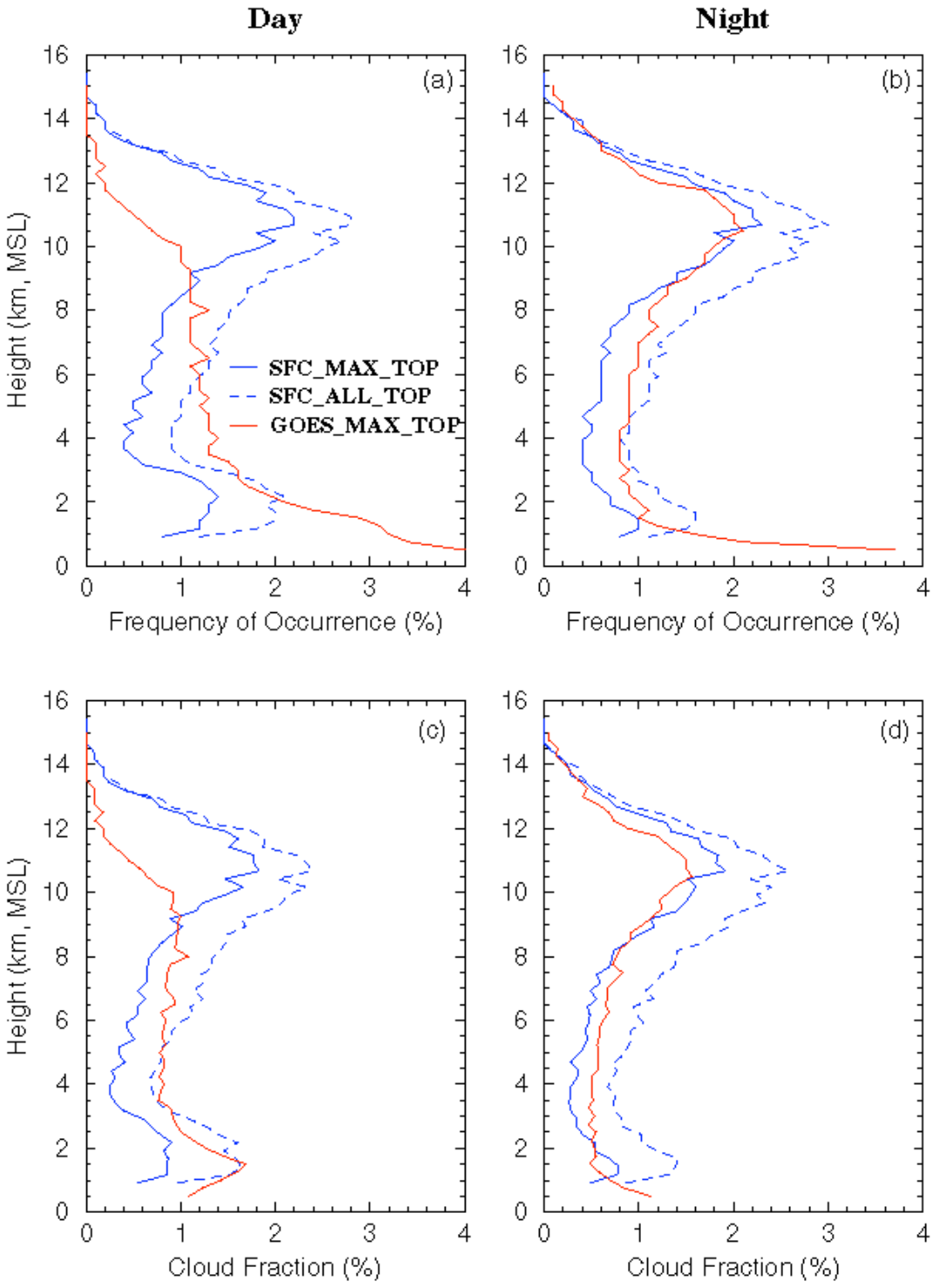

287

288 Figure 3.